Modelling of MILD combustion in a lab-scale furnace with an extended FGM model including turbulence–radiation interaction

Huang, Xu; Tummers, Mark J.; van Veen, Eric H.; Roekaerts, Dirk J.E.M.

DOI
10.1016/j.combustflame.2021.111634

Publication date
2022

Document Version
Final published version

Published in
Combustion and Flame

Citation (APA)
Huang, X., Tummers, M. J., van Veen, E. H., & Roekaerts, D. J. E. M. (2022). Modelling of MILD combustion in a lab-scale furnace with an extended FGM model including turbulence–radiation interaction. *Combustion and Flame*, *237*, Article 111634. https://doi.org/10.1016/j.combustflame.2021.111634

Combustion and Flame 237 (2022) 111634

Contents lists available at ScienceDirect

Combustion and Flame

journal homepage: www.elsevier.com/locate/combustflame

Modelling of MILD combustion in a lab-scale furnace with an extended FGM model including turbulence–radiation interaction

Xu Huang[a,b,*], Mark J. Tummers[b], Eric H. van Veen[b], Dirk J.E.M. Roekaerts[b,c]

[a] *China Aerodynamics Research and Development Centre, NO. 6, South Section, 2nd Ring Road, Mianyang, China*
[b] *Department of Process and Energy, Delft University of Technology, Leeghwaterstraat 39,Delft 2628 CB, the Netherlands*
[c] *Department of Mechanical Engineering, Eindhoven University of Technology, P.O Box 513, Eindhoven 5600 MB, the Netherlands*

ARTICLE INFO

Article history:
Received 31 August 2020
Revised 22 July 2021
Accepted 23 July 2021

Keywords:
MILD Combustion
Modelling
Dilution effects
Turbulence–radiation interaction
OpenFOAM

ABSTRACT

The flamelet generated manifold (FGM) model is suitable for moderate or intense low oxygen dilution (MILD) combustion provided the flamelets underlying the manifold include the effects of strong dilution by products of the fuel/oxidizer mixture. Here we propose such an extended model based on the use of non-premixed flamelets diluted at the airside and develop its application to non-adiabatic combustion in a lab-scale furnace. The extended model is referred to as diluted air FGM (DA-FGM) model. In the DA-FGM model in addition to mixture fraction, progress variable and scaled enthalpy loss, one additional controlling parameter named air dilution level, is introduced leading to a four-dimensional lookup table for laminar flames. For turbulent flames also variances of mixture fraction and progress variable are taken into account as independent variables leading to a six-dimensional table. Using a RANS approach implemented in OpenFOAM-2.3.1, the DA-FGM model has been applied to MILD combustion of Dutch natural gas in a lab-scale furnace operated at a thermal power 9 kW and at equivalence ratio 0.8. Radiation is described using a weighted-sum-of-gray-gases (WSGG) model. The validation study is mainly done using a grey WSGG model with TRI taken into account. The relative importance of including turbulence radiation interaction (TRI) and spectral treatment of radiative transfer is also studied. The predicted velocity and temperature statistics are in good agreement with the experimental LDA and CARS data provided not only the mixture fraction fluctuations but also the progress variable fluctuations are taken into account.

1. Introduction

Models for turbulence–chemistry interaction in MILD or flameless combustion should represent the actual flame structure to the extent that they provide an accurate prediction of the mean reaction rates. Detailed fundamental information on the flame structure under the influence of dilution by combustion products is available from local experiments and from Direct Numerical Simulation (DNS). Recent DNS studies by Minamoto and Swaminathan [1] have revealed that for a well-defined case of combustion in the presence of dilution, a structure dominated by interactions between thin reaction zones can occur. The DNS results also suggested that, depending on the dilution level, the interaction between the thin reaction zones varies; that is, sustained interaction between the thin reaction zones occurs at high dilution levels, while little interaction occurs at a low dilution level. High-speed chemiluminescence measurements in the TU Delft lab-scale MILD combustion furnace have made clear that the reacting flow with increasing distance from the burner successively enters regimes with isolated ignition kernels, ignition kernel clusters and fully connected reaction zones [2]. This observation provides experimental evidence for the role of interactions between flame structures.

In the RANS and LES approaches to turbulent combustion the local transient interactions cannot be resolved, but instead, a model to calculate the mean or resolved source terms is used. Minamoto and Swaminathan [1] have investigated how well the mean reaction rates in their DNS of MILD combustion are described by three "paradigms": standard flamelets based on pure fuel and pure oxidizer, flamelets based on diluted streams ("mild flame elements"), and a perfectly stirred reactor (PSR) with the size of the laminar flame thickness (thermal thickness or Zeldovich thickness). They concluded that the pure fuel and pure air flamelets are not suitable, that the diluted flamelets give qualitative agreement and the PSR-based model is appropriate.

---

[*] Corresponding author at: China Aerodynamics Research and Development Centre, NO. 6, South Section, 2nd Ring Road, Mianyang, China.
E-mail address: huangxu219@163.com (X. Huang).

https://doi.org/10.1016/j.combustflame.2021.111634

A very wide range of RANS and LES approaches has been applied to MILD combustion in jet in hot coflow configurations (mimicking MILD combustion using a simple flow configuration) and in furnaces. These have been reviewed by Perpignan et al. [3]. Models based on a chemical reactor involving many chemical time scales often have been used in a mixing process between reaction zone and surroundings at a rate dominated by one time scale. In this category fall the Eddy Dissipation Concept (EDC) model and the closely related partially stirred reactor (PaSR) models. In these models the large-scale effects of dilution by product species are calculated explicitly because mean transport equations for all species are solved without the local effects of dilution resolved, but represented by the reactor based closure model.

RANS models combining standard turbulence models and several chemical mechanisms with the EDC model have been applied to several lab-scale MILD furnaces, see e.g. [4–7]. It has been found that the accuracy of the predictions can be improved by adjusting model constants from their standard values optimized for regular combustion in non-diluted conditions. Approaching this model adjustment from a more fundamental point of view, Parente et al. [8] developed an extended EDC model (E-EDC) in which the model constants are depending on local conditions characterized by turbulence Reynolds number and Damköhler number. In this way the model was made capable of qualitatively taking into account the expected type of local flame structure. Recently a new version of the extended EDC model (NE-EDC) was derived by Romero-Anton et al. [9] and validated by application to the TU Delft lab-scale MILD furnace [2,10]. They compared E-EDC, NE-EDC and a flamelet generated manifold (FGM) model using flamelets from counterflowing pure fuel and pure air streams. The NE-EDC was found to give the best prediction. Nevertheless, the predictions of NE-EDC for MILD combustion in this furnace are not as good as the predictions that can be obtained using an FGM based on diluted flamelets, that have been reported earlier in Refs[2,10]. and that are elaborated in this article. Before introducing this model in more detail we first review some relevant previous works.

Several authors have proposed tabulated chemistry methods for combustion in situations with dilution by combustion products. The first aspects to be addressed are the way to characterize the level of dilution with product gases and the way to include this representation in a tabulated chemistry model. In the framework of flamelet models the dilution is imposed at the fuel and/or oxidizer boundary conditions. The effects of dilution by combustion products on non-premixed counterflow flamelets were studied by Abtahizadeh et al. [11]. The level of dilution of the fuel and/or air stream in a counterflow configuration was found to be a dominant parameter to control chemical effects whereas strain rate was found the most important parameter to control diffusion effects. Abtahizadeh et al. [11] did not make the step to utilization of the diluted flamelets in simulations of a turbulent combustion system. In order to do so it is necessary to define algorithms to handle dilution and heat loss and a look-up table, which is investigated in the present article.

First applications of tabulated chemistry to a MILD furnace were made by Locci et al. [12,13], Lamouroux et al. [14] and Colin and Michel [15]. They all validated their models with the experiments by Veríssimo et al. [16] on combustion in a cylindrical furnace in Technical University of Lisbon. The burner in that case is located in the bottom plane and injects reactants via a central air jet surrounded by a number of fuel jets. This furnace has been simulated earlier using EDC in RANS [4,5]. In the works by Locci et al. and by Lamouroux et al. the lookup table was integrated in a Large Eddy Simulation. To construct the tabulated chemistry, Locci et al. used diluted homogeneous reactors instead of diluted flamelets. These reactors capture the autoignition phenomena as function of dilution levels and enthalpy loss. Effects of strain rate variations in the flow in the representation by homogeneous reactors are represented by variations in residence time. Lamouroux et al. proposed an extension of the flamelet progress variable (FPV) approach. Their library was generated by laminar counterflow flames using diluted fuel and diluted air at the same dilution levels (mass fraction of diluent). The diluent was considered to be the flue gas corresponding to the actual overall equivalence ratio during the furnace operation.

Colin and Michel [15] developed a two-dimensional flamelet equation using the FPI/FGM approach in order to account for the three-stream mixing that occurs between air, fuel and burnt gases. This equation is not solved for all species present in the chemical mechanism, but only for the progress variable. The enthalpy loss is included in the model as a pre-defined parameter. The diluent was taken to be the flue gas at the overall stoichiometry of the furnace operation.

Another MILD combustion furnace was designed and built at the university of Naples (Sorrentino et al. [17]). The injection strategy for creating the conditions for MILD combustion is completely different from the strategy used in the furnaces of Lisbon and Delft that are using parallel jets of fuel and preheated oxidizer. Separate tangentially injected fuel and air jets at opposite sides driving a cyclonic flow in the combustor create the conditions necessary for MILD combustion. Sorrentino et al. [17] reported experimental results and numerical simulations using a perfectly stirred reactor model. Chen et al. [18] extended the numerical study using the PSR and concluded that the mean temperature was well-predicted provided the non-adiabatic effects were taking into account. A step further in the modelling of this system was made by Ceriello et al. [19] using tabulated chemistry method (FGM). In their work two configurations of flame structures used for creating the FGM were compared: FGM based on igniting mixing layer (non-premixed) between pure fuel and pure oxidizer and FGM based on premixed flamelets. They found that the configuration used to create the manifold did not affect the simulation in a strong way. For some regions in the furnace the mean temperature was consistently overestimated. Apart from modelling of turbulence–chemistry interaction also modelling of convective and radiative heat transfer in the furnace is important. The turbulence models for momentum and scalar transport provide the prediction of turbulent convective heat transfer. The radiative heat transfer equation describes the transport of energy by radiation. However, turbulence and radiation mutually influence each other. This is known as turbulence radiation interaction (TRI) and is also to be properly represented. The temperature field is influenced by TRI, as well as all quantities (e.g. species) that are affected by temperature. Therefore, a better modelling of thermal radiation, taking TRI into account, may improve the prediction of the temperature field, flame structure, and pollutants emission [20]. Consideration of the temperature self-correlation alone is not sufficient to determine turbulence–radiation interactions [21,22]. In this article TRI will be included by exploiting all available information from the statistical description of the turbulence–chemistry interaction model, namely the assumed PDF method for mixture fraction and progress variable in the context of diluted air FGM tabulated chemistry. The spectral treatment of radiation is another aspect of importance. In the present work we mainly use a standard gray treatment of radiation. The importance of including spectral treatment is studied in a small complementary study.

The FGM-based model for MILD combustion used in this work differs from all the tabulated chemistry models described above. Firstly, it uses as diluent the products of stoichiometric combustion instead of products at the global conditions of the furnace operations. Secondly, it employs counterflow diffusion flamelets based on undiluted fuel and diluted air. This diluted air FGM model is denoted by the acronym DA-FGM and is described in detail in

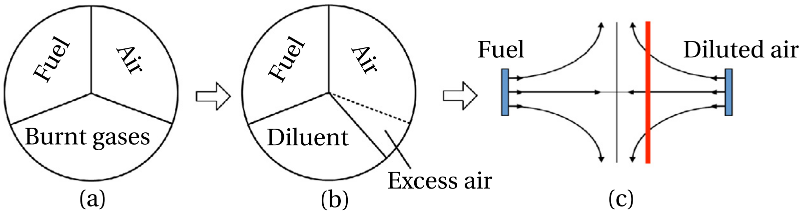

Fig. 1. Schematic of representative mixture components in the furnace with strong internal recirculation. (a) and (b) illustrate the definition of diluent; (c) illustrates the addition of diluent in a counterflow flame configuration.

Section 2.1. The model was implemented in the open source CFD package OpenFOAM, version 2.3.1. A detailed explanation of the DA-FGM tabulated chemistry method is given in Section 2.1, including model description, library generation and lookup procedure. The method for handling TRI and its coupling with the DA-FGM model is described in Section 2.2. The experimental setup is presented in Section 3. Computational setup and flamelets generation are described in Section 4. The validation of the model comparison with experimental measurements in the Delft lab-scale MILD furnace is presented in Section 5.

2. Modelling approach

2.1. Diluted air FGM (DA-FGM) model

The Flamelet Generated Manifold (FGM) method simplifies the description of the local thermochemical states in a flame by assuming that the relations between properties are the same as the relations found in a set of laminar flames, including the chemical source terms for one or more progress variables. Full specification of an FGM therefore requires the selection of a representative set of laminar flames and the selection of the progress variable. In the case of MILD combustion the local states are highly influenced by dilution of the product gases and it is necessary to take this into account in the selection of the representative laminar flames.

2.1.1. Definition of diluent

The reacting flow structure in MILD combustion can be considered to be arising from a mixture of fuel, air and burnt gases. A schematic of these mixture components is shown in Fig. 1(a). For a furnace operating at global equivalence ratio $\phi = 1$, the burnt gases recirculated to the reaction zone are the products at stoichiometric mixture fraction Z_{st}. Assuming a sufficiently long residence time in the furnace the recirculated gas can be assumed to be in chemical equilibrium. In this case, there is no excess air left in the burnt gases and the recirculated gas essentially acts as an inert diluent. However, when a furnace is operating at a lean condition or global equivalence ratio $\phi < 1$, excess air is left in the burnt gases and the recirculated gas is reactive. The burnt gases at $\phi < 1$ is not an inert diluent, but also contains oxygen. This leads to complications in the formulation of a diluted FGM model.

Previous works using diluted flamelets [12–14] have defined the diluent stream as burnt gases at global equivalence ratio determined by the furnace operation. As mentioned, because the flue gas contains a significant fraction of oxygen, the fuel may react with the oxygen in the entrained products before it mixes with the fresh air stream. Furthermore, in the tabulation method in Ref.[14]., both the fuel and the air are diluted and the mass fractions of the diluent in the diluted fuel and the diluted air are assumed to be the same. The flamelets have the diluted fuel and the diluted air as boundary condition. In this way, only the mixing state between fuel and diluent is tabulated in the table and a possible reaction between fuel and diluent is not included. Moreover, the mixing and reacting states between the fuel and a mixture in which the oxygen mass fraction is lower than that in burnt gases are not included in the library, either. To avoid these limitations we here propose to use for the FGM creation a diluent that is defined as products of stoichiometric combustion, as explained in more detail below.

The fact that we introduce a diluent not containing oxygen does not mean that we cannot describe furnace operation at lean conditions. To represent the physical states expected from recirculation of a product stream of lean combustion, it is necessary to note that every state of mixing between air and flue gas can be mapped on a state of mixing between air and products of stoichiometric combustion. It is sufficient to consider any flue gas from lean combustion as a mixture of flue gas from stoichiometric combustion and excess air, and to combine the air and the excess air. The local combustion process is then represented by the laminar counterflow diffusion flames between fuel and diluted air with as diluent the products of stoichiometric combustion. See Figs. 1(b,c). It leads to a simple characterization of the laminar flames to be considered because they are based on three well-defined streams, fuel, air and equilibrium products of stoichiometric combustion. The question that will have to be addressed in the application of the FGM to a furnace is the determination of the level of diluent based on the information available on the local conditions in the furnace.

2.1.2. Flamelets with dilution

The state of mixing of the counterflow flamelets is characterised by two variables. The first one is the mass fraction of diluent in the diluent/air mixture, called air dilution level and denoted by γ. The second one is the mixture fraction associated with the mixing of fuel and diluted air, denoted by ξ. Flamelets are calculated using the laminar diffusion counterflow configuration in Fig. 1(c) with the following boundaries:

$$\Phi(\xi = 1) = \Phi_f, \tag{1}$$

$$\Phi(\xi = 0) = \Phi_{ox}(\gamma), \tag{2}$$

where Φ_f and Φ_{ox} are respectively pure fuel state and diluted air state. An FGM based on adiabatic flamelets will be three-dimensional, namely the properties are depending on ξ, C and γ

$$\Phi = \Phi_3(\xi, C, \gamma). \tag{3}$$

where C is the progress variable. Determination of the value of these parameters from local conditions in an application to a MILD combustion furnace will be addressed in the Section 2.1.4.

2.1.3. Non-adiabatic flamelet library with dilution

To take into account enthalpy loss effects, the diluent is considered to have an enthalpy deficit compared to the adiabatic case. That is, air is diluted by an amount of burnt gases at Z_{st} having an enthalpy loss dh. This dh includes both enthalpy loss due to radiation and heat transfer to the cold walls. Since the diluent is only present at the air side, enthalpy loss does not have impact on the fuel side of the counterflow flame configuration. The boundary conditions for the counterflow flames now read:

$$\Phi(\xi = 1) = \Phi_f, \tag{4}$$

$$\Phi(\xi = 0) = \Phi_{ox}(\eta, \gamma), \tag{5}$$

where the enthalpy loss factor η is a normalized enthalpy loss, with $\eta = 0$ and $\eta = 1$ corresponding respectively to minimum and maximum enthalpy loss. Determination of the enthalpy loss factor η is described in the next subsection. The dependent thermochemical properties in the FGM now depend on four independent variables:

$$\Phi = \Phi_4(\xi, C, \eta, \gamma). \tag{6}$$

2.1.4. Lookup procedure

In order to use the tabulated data in the four-dimensional table, the controlling parameters, ξ, C, η and γ must be determined from local conditions in the furnace. The controlling variables are not solved directly from transport equations, but they are derived from other variables as follows.

The calculation of the combustion in the furnace makes use of the mixture fraction describing the mixing between the fuel and air streams entering the furnace from the burner. This mixture fraction is denoted by Z. But by assumption of the DA-FGM model the mixture is considered to be a state in a flamelet constructed with fuel and diluted air as inlet streams, rather than a flamelet constructed with fuel and air as inlet streams. By definition the diluent has a value of mixture fraction Z_{st}. The mass fraction of the diluent in the mixture of fuel, air and diluent is denoted α. The mass fraction of the fuel and air streams in the mixture is $1 - \alpha$. The mixture fraction Z of the local instantaneous gas mixture is then given by

$$Z = (1 - \alpha)Z_0 + \alpha Z_{st}, \tag{7}$$

where Z_0 is the mixture fraction of fuel-air mixture. Here Z, Z_0 and Z_{st} are all based on pure fuel and pure air.

The relation between α and the dilution level of the oxidizer in the flamelets is

$$\alpha = \gamma(1 - \xi) \tag{8}$$

Determination of dilution level α

In the combustion in the furnace, dilution is caused by internal recirculation of combustion products. The local effects of this are accounted for by representing the combustion process as combustion in a flamelet with diluted inflow conditions. In the flamelet states, this is described by two strictly related quantities, the fraction of diluent at the air side of the flamelet (γ) and the fraction of diluent in the mixture (α). When the DA-FGM table is used to retrieve the full thermochemical composition in the furnace, first the value of α is calculated. In order to do so, an extra transport equation is solved for a quantity Y_d providing information on recirculated products. Y_d represents mass fraction of species products present in fully burnt states. The normalised value of Y_d, relative to its value in products of complete combustion is equal to α. Here the dilution variable is based on $Y_d = Y_{CO_2} + Y_{H_2O}$, and the relation between Y_d and α is

$$\alpha = \frac{Y_d}{Y_d^{Dil}}, \tag{9}$$

Here Y_d^{Dil} denotes the value of Y_d in the dilution stream which consists of burnt gases at stoichiometric mixture fraction Z_{st}.

At any location in the furnace, the full thermochemical state is retrieved from the DA-FGM table by taking into account the value of α (and other independent scalars). There are of course some assumptions underlying this procedure, the most important one is the assumption that the heat release zones in the furnace are well represented by diluted flamelets. Our model is based on specific assumptions (dilution with products of complete combustion; dilution of flamelets at the oxidizer side). Generally speaking, this method is expected to be very accurate when the actual recirculation returns products of complete combustion to the mixture that is flowing towards a reaction zone. But we point out that it is also appropriate when the recirculation in the furnace still has some oxygen content (lean combustion). By taking into account the value of mixture fraction, it is made sure that the oxygen balance in the flame zone is fully respected when retrieving data from the flamelet library.

Determination of the second mixture fraction ξ and air dilution level γ

The mixture fraction in the counterflow flame calculations is ξ. It is related to the mixture fraction based on fuel and air via

$$\xi = Z - \alpha Z_{st} = (1 - \alpha)Z_0, \tag{10}$$

and the mass fraction of diluent in diluted air, needed for lookup, is given by

$$\gamma = \frac{\alpha}{1 - \xi} = \frac{\alpha}{1 - Z + \alpha Z_{st}}. \tag{11}$$

Determination of enthalpy loss factor η

Once air dilution level is obtained, enthalpy loss factor η can be determined. Enthalpy loss Δh is normalized by the maximum tabulated enthalpy loss at local dilution level which results in η. The local maximum enthalpy is $\gamma(1 - \xi)\left(h^d_{\eta=1} - h^d_{\eta=0}\right)$. η is therefore expressed as

$$\eta = \frac{\Delta h}{\gamma(1 - \xi)\left(h^d_{\eta=1} - h^d_{\eta=0}\right)} = \frac{h - h_{ad}}{\alpha\left(h^d_{\eta=1} - h^d_{\eta=0}\right)}, \tag{12}$$

where h_{ad} is the adiabatic enthalpy at local mixture fraction

$$h_{ad} = Zh_f + (1 - Z)h_{ox}, \tag{13}$$

$h^d_{\eta=1}$ and $h^d_{\eta=0}$ are respectively the enthalpy of diluent with maximum and minimum enthalpy loss. The minimum enthalpy loss usually is zero, and the maximum enthalpy loss has to be specified based on the information of the specific application. To calculate the value of η, the value of Z (entering h_{ad}) and h are needed.

Determination of scaled progress variable C

Progress variable is defined as the sum of a selected number of species mass fractions

$$Y_c = \sum_{k=1}^{N_{Y_c}} Y_k. \tag{14}$$

The key factor on progress variable definition is that in a flamelet it defines the combustion unambiguously. In this study the following choice is made

$$Y_c = Y_{CO_2} + Y_{CO} + Y_{H_2O} + Y_{H_2}. \tag{15}$$

From the progress variable, the corresponding scaled progress variable used in the tabulation can be calculated provided the minimum and maximum values of the progress variable also have been stored in the lookup table. In the case of undiluted flamelets it is already the case that the minimum and maximum values of a progress variable depend on the mixture fraction. Now the minimum and maximum values will also depend on the enthalpy loss and on the air dilution level, because the oxidizer side of flamelets contains the species that are taken into account in the definition of the progress variable and the states that are reached depend on the enthalpy. Taking this into account, the scaled progress variable C is obtained as

$$C = \frac{Y_c - Y_c^u(\xi, \eta, \gamma)}{Y_c^b(\xi, \eta, \gamma) - Y_c^u(\xi, \eta, \gamma)}, \tag{16}$$

where Y_c^u and Y_c^b are respectively the value of Y_c in unburnt state and burnt state.

In summary, four controlling parameters ξ, C, η and γ are defined by Eqs. (10), (16), (12) and (11) respectively.

2.1.5. Tabulation of averaged quantities

In the context of a RANS simulation the scalar variables are considered to be fluctuating and characterised by a joint scalar PDF. For simplicity we here consider that only the fluctuations of mixture fraction and of progress variable have to be taken into account and that the mixture fraction and the scaled progress variable are statistically independent. A presumed β-PDF for mixture fraction and scaled progress variable is used.

The mean properties can be calculated based on the joint PDF of ξ, C, η and γ, and it is assumed that they are statistically independent

$$\widetilde{\Phi} = \int_0^1 \int_0^1 \int_0^1 \int_0^1 \Phi(\xi, C, \tilde{\eta}, \tilde{\gamma}) \widetilde{P}(\xi) \widetilde{P}(C) d\xi dC d\eta d\gamma. \tag{17}$$

The mean properties are stored in a six-dimensional lookup table

$$\widetilde{\Phi} = \Phi_6\big(\widetilde{\xi}, S_\xi, \widetilde{C}, S_C, \widetilde{\eta}, \widetilde{\gamma}\big). \tag{18}$$

where where S_ξ and S_C are the normalized variance of ξ and C, called the segregation factor, and are defined by Eqs. (35) and (37) respectively.

In an optional further simplification, the fluctuations in progress variable are neglected and then the progress variable variance equation does not have to be solved and the mean properties are stored in a five-dimensional table.

$$\widetilde{\Phi} = \Phi_5\big(\widetilde{\xi}, S_\xi, \widetilde{C}, \widetilde{\eta}, \widetilde{\gamma}\big). \tag{19}$$

2.1.6. Lookup in RANS simulation

Favre-averaged transport equations are solved for mixture fraction $\widetilde{Z}$, progress variable $\widetilde{Y_c}$, dilution variable $\widetilde{Y_d}$ and enthalpy $\widetilde{h}$, mixture fraction variance $\widetilde{Z''^2}$ and progress variable variance $\widetilde{Y_c''^2}$.

$$\frac{\partial \bar{\rho}\widetilde{Z}}{\partial t} + \frac{\partial}{\partial x_i}\big(\bar{\rho}\widetilde{u}_i\widetilde{Z}\big) = \frac{\partial}{\partial x_i}\left[\bar{\rho}\big(\widetilde{D} + D_t\big)\frac{\partial \widetilde{Z}}{\partial x_i}\right], \tag{20}$$

$$\frac{\partial \bar{\rho}\widetilde{Y_c}}{\partial t} + \frac{\partial}{\partial x_i}\big(\bar{\rho}\widetilde{u}_i\widetilde{Y_c}\big) = \frac{\partial}{\partial x_i}\left[\bar{\rho}\big(\widetilde{D} + D_t\big)\frac{\partial \widetilde{Y_c}}{\partial x_i}\right] + \bar{\dot{\omega}}_{Y_c}, \tag{21}$$

$$\frac{\partial \bar{\rho}\widetilde{Y_d}}{\partial t} + \frac{\partial}{\partial x_i}\big(\bar{\rho}\widetilde{u}_i\widetilde{Y_d}\big) = \frac{\partial}{\partial x_i}\left[\bar{\rho}\big(\widetilde{D} + D_t\big)\frac{\partial \widetilde{Y_d}}{\partial x_i}\right] + \bar{\dot{\omega}}_{Y_d}, \tag{22}$$

$$\frac{\partial \bar{\rho}\widetilde{h}}{\partial t} + \frac{\partial}{\partial x_i}\big(\bar{\rho}\widetilde{u}_i\widetilde{h}\big) = \frac{\partial}{\partial x_i}\left[\bar{\rho}\big(\widetilde{D} + D_t\big)\frac{\partial \widetilde{h}}{\partial x_i}\right] + \bar{S}_r, \tag{23}$$

$$\begin{aligned}&\frac{\partial \bar{\rho}\widetilde{Z''^2}}{\partial t} + \frac{\partial}{\partial x_i}\big(\bar{\rho}\widetilde{u}_i\widetilde{Z''^2}\big)\\ &= \frac{\partial}{\partial x_i}\left[\bar{\rho}\big(\widetilde{D} + D_t\big)\frac{\partial \widetilde{Z''^2}}{\partial x_i}\right] + 2\bar{\rho}D_t\left(\frac{\partial \widetilde{Z}}{\partial x_i}\right)^2 - \bar{\rho}\,\widetilde{\chi}_Z,\end{aligned} \tag{24}$$

$$\begin{aligned}&\frac{\partial \bar{\rho}\widetilde{Y_c''^2}}{\partial t} + \frac{\partial}{\partial x_i}\left(\bar{\rho}\widetilde{u}_i\widetilde{Y_c''^2}\right)\\ &= \frac{\partial}{\partial x_i}\left[\bar{\rho}\big(\widetilde{D} + D_t\big)\frac{\partial \widetilde{Y_c''^2}}{\partial x_i}\right] + 2\bar{\rho}D_t\left(\frac{\partial \widetilde{Y_c}}{\partial x_i}\right)^2\\ &- \bar{\rho}\,\widetilde{\chi}_{Y_c} + 2\Big(\overline{Y_c\dot{\omega}_{Y_c}} - \widetilde{Y_c}\bar{\dot{\omega}}_{Y_c}\Big).\end{aligned} \tag{25}$$

The turbulent scalar dissipation rate for mixture fraction and progress variable variance $\bar{\rho}\widetilde{\chi}_Z$ and $\bar{\rho}\widetilde{\chi}_{Y_c}$ in Eqs. (24) and (25) are respectively modelled as follows [23]:

$$\widetilde{\chi}_Z = C_{Zv}\frac{\epsilon}{k}\widetilde{Z''^2}, \tag{26}$$

and

$$\widetilde{\chi}_{Y_c} = C_{Y_c v}\frac{\epsilon}{k}\widetilde{Y_c''^2}, \tag{27}$$

with model constants $C_{Zv} = 2$, $C_{Y_c v} = 2$. Turbulence is modelled with a standard $k - \epsilon$ model. The turbulent Schmidt number and turbulent Prandtl number are both 0.7.

The source terms in Eqs. (21) and (25), $\bar{\dot{\omega}}_{Y_c}$ and $\overline{Y_c\dot{\omega}_{Y_c}}$ are tabulated in the lookup table. The radiation source term $\bar{S}_r$ in Eq. (23) is calculated by the radiation model but its essential parts are also included in the lookup table (see Section 2.2).

Eq. (22) for dilution variable shows that the local value of $\widetilde{Y_d}$ is determined by several processes: a source term describing change in the level of dilution by the appearance of fully burnt mixture and transport by convection and diffusion. The source term is given by

$$\bar{\dot{\omega}}_{Y_d} = \frac{1}{\Delta t}\bar{\rho}\left(\widetilde{Y_d^b} - \widetilde{Y_d}\right)H(\widetilde{C} - 0.99), \tag{28}$$

The source term describes a very relaxation of the mean dilution variable to $\widetilde{Y_d^b}$, the mean dilution variable in local burnt gases, at a fast rate set by Δt is the simulation time step. It should be pointed out that $\widetilde{Y_d^b}$ is depending on the local mixture fraction. This relation is also stored in the lookup table: $\widetilde{Y_d^b} = Y_d^b\big(\widetilde{\xi}, S_\xi, \widetilde{\eta}, \widetilde{\gamma}\big)$ at $\widetilde{C} = 1$. The H function is a unit step function which is used to activate the source term when fully burnt mixture is present (characterised by c being higher than the value 0.99). The source term does not contain chemical reaction rates for fuel species since the chemical evolution of product species has been calculated in the flamelets. The function of the source term in the equation for dilution variable is only to control the shift in the applicable flamelet states.

With the solutions from the transport equations discussed above, the table lookup controlling parameters can be derived.

$$\widetilde{\alpha} = \frac{\widetilde{Y_d}}{Y_d^{Dil}}, \tag{29}$$

$$\widetilde{\xi} = \widetilde{Z} - \widetilde{\alpha}Z_{st}, \tag{30}$$

$$\widetilde{\gamma} = \frac{\widetilde{\alpha}}{1 - \widetilde{\xi}}, \tag{31}$$

$$\widetilde{\eta} = \frac{\widetilde{h} - \widetilde{h}_{ad}}{\widetilde{\alpha}\left(h^d_{\eta=1} - h^d_{\eta=0}\right)}, \tag{32}$$

$$\widetilde{C} = \frac{\widetilde{Y_c} - \widetilde{Y_c^u}}{\widetilde{Y_c^b} - \widetilde{Y_c^u}}. \tag{33}$$

S_ξ is determined by assuming no fluctuations for Y_d, and therefore α is not fluctuating. Using Eqs. (10) and (30), the following equations are obtained

$$\widetilde{\xi''^2} = \widetilde{Z''^2}, \tag{34}$$

$$S_\xi = \frac{\widetilde{\xi''^2}}{\widetilde{\xi}(1 - \widetilde{\xi})} = \frac{\widetilde{Z''^2}}{(\widetilde{Z} - \widetilde{\alpha}Z_{st})(1 - \widetilde{Z} + \widetilde{\alpha}Z_{st})}. \tag{35}$$

S_C can be determined by following the formula in [24,25]

$$\widetilde{C''^2} = \frac{\widetilde{Y_c''^2} - \left(\widetilde{Y_c}\right)^2 - \widetilde{(Y_c^u)^2} - 2\widetilde{C}\left[\widetilde{Y_c^u Y_c^b} - \widetilde{(Y_c^u)^2}\right]}{\left(\widetilde{Y_c^b} - \widetilde{Y_c^u}\right)^2} - \widetilde{C}^2, \tag{36}$$

$$S_C = \frac{\widetilde{C''^2}}{\widetilde{C}(1-\widetilde{C})}, \tag{37}$$

where $\left(\widetilde{Y}_c\right)^2$, $\widetilde{(Y_c^u)^2}$ and $\widetilde{Y_c^u Y_c^b}$ are pre-integrated and tabulated as functions of $\widetilde{\xi}$, $\widetilde{\xi''^2}$, $\widetilde{\eta}$ and $\widetilde{\gamma}$.

2.2. Radiative heat transfer modelling

Modelling of radiative heat transfer consists of specification of a model for radiative properties, a solution method for the mean radiative transfer equation (RTE), a closure for the unclosed terms due to Reynolds averaging and the evaluation of the mean radiative source term in the enthalpy equation Eq. (23).

2.2.1. Radiative properties

Scattering can be neglected in a gas fired furnace and only the effects of absorption and emission must be represented. Here we simply use a grey treatment for radiation. The grey gas absorption coefficient is calculated from a weighted-sum-of-grey-gas (WSGG) model with four grey gases (J=4) and one clear gas. The coefficients proposed by R. Johansson et al. [26] are adopted to account for various ratios of H_2O to CO_2 concentrations. The grey absorption coefficient is used when solving the RTE for the total intensity. The question how large the sensitivity of the predictions is on the use of grey radiation treatment instead of the more accurate spectral radiation transfer is addressed in Section 5.5. In the grey treatment, following the traditional approach of Hottel and Sarofim [27], an effective absorption coefficient deduced from total emissivity is calculated from

$$\kappa = -\frac{\ln(1-\varepsilon)}{s}, \tag{38}$$

where s is taken to be the mean beam length

$$s = \frac{3.6V}{A}, \tag{39}$$

Here V is the volume of the domain and A the corresponding surface area. It is used when directly solving the RTE for the total intensity. A more accurate prediction of heat flux and radiative source term can be achieved by solving an RTE for each of the grey gases. This will be elaborated further in Section 5.5.

2.2.2. RTE with turbulence–radiation interaction (TRI)

In the case of a grey gas, the radiative transfer equation (RTE) for an absorbing, emitting, and non-scattering medium takes the form [28]:

$$\frac{\partial}{\partial x} I(\mathbf{r},\mathbf{s})s = -\kappa(\mathbf{r})I(\mathbf{r},\mathbf{s}) + \kappa(\mathbf{r})I_b(\mathbf{r}). \tag{40}$$

In the above equation, $I(\mathbf{r},\mathbf{s})$ is the total radiation intensity at point $\mathbf{r}$ and direction $\mathbf{s}$, I_b is the total blackbody radiation intensity, κ is the absorption coefficient of the medium. A numerical solution of the equation is calculated using the Discrete Ordinates Method (DOM). In this study, each octant of the angular space 4π at any spatial location is discretized into 2×2 solid angles. Hence, a total of 32 directional intensities I^m are calculated where the superscript m stands for one of the directions resulting from the angular discretization [29].

The time-averaged form of the RTE (Eq. (40)) contains averages of nonlinear terms that are unclosed which is denoted as TRI. A comprehensive review of closure methods for the terms is given in Ref. [30]. In the case of gas fired furnaces the optically thin fluctuation approximation (OTFA) can be made. It says that the values of absorption coefficient and radiative intensity are uncorrelated [31]. Then the mean RTE takes the form

$$\frac{\partial}{\partial x}\overline{I^m}s = -\overline{\kappa}\,\overline{I^m} + \overline{\kappa I_b}, \tag{41}$$

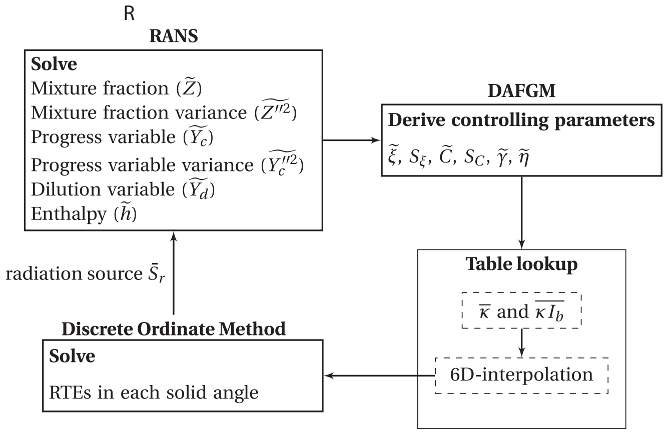

Fig. 2. Schematic of the data exchange between scalar transport equations, radiative transfer model and tabulated chemistry.

The time-averaged terms $\overline{\kappa}$ and $\overline{\kappa I_b}$ depend on the statistical properties of the local species concentrations and temperature. In the framework of the DA-FGM model for local composition they can be expressed in closed form using Eq. (18) [20].

$$\overline{\kappa} = \overline{\rho}\int_0^1\int_0^1\int_0^1\int_0^1 \frac{\kappa(\xi,C,\eta,\gamma)}{\rho(\xi,C,\eta,\gamma)}\widetilde{P}(\xi,C,\eta,\gamma)\,d\xi\, dC\, d\eta\, d\gamma, \tag{42}$$

$$\overline{\kappa I_b} = \frac{\overline{\rho}\pi}{\sigma}\int_0^1\int_0^1\int_0^1\int_0^1 \frac{\kappa(\xi,C,\eta,\gamma)T^4(\xi,C,\eta,\gamma)}{\rho(\xi,C,\eta,\gamma)}\widetilde{P}(\xi,C,\eta,\gamma)\,d\xi\, dC\, d\eta\, d\gamma. \tag{43}$$

Only these two additional terms need to be stored in the lookup table instead of mean temperature, mean mole fractions and mean powers of temperature. During the simulation, controlling parameters for library lookup are obtained, and the above two terms are then retrieved from the library.

2.2.3. Coupling radiation with combustion

When the radiation intensities in each discrete ordinate direction are obtained the radiation source term in the enthalpy equation is given by

$$\nabla\cdot\mathbf{q} = 4\pi\overline{\kappa I_b} - \sum_{m=1}^{M}\omega_m\overline{I^m}, \tag{44}$$

where ω_m is the weight for the mth direction.

The complete coupling strategy is depicted in Fig. 2 with arrows representing transfer of values of relevant quantities. In order to reduce the total computational time, first a simulation was made without taking radiative heat transfer into account. Once a converged combustion field was obtained, radiation was switched on. Ten iterations of the flow solver are followed by one integration of the radiation solver. All fields are updated until the steady fields are obtained.

3. Experimental configuration and database

3.1. Experimental configuration

The experiments used for model validation were done in a lab-scale furnace at Delft University of Technology. A schematic of the furnace is displayed in Fig. 3. It consists of a WS REKUMAT 150 recuperative Flame-FLOX burner and a thermally insulated, but optically accessible, combustion chamber with internal dimensions of 320 mm×320 mm×630 mm. The burner and internal top wall can be moved in the vertical direction relative to the fixed side

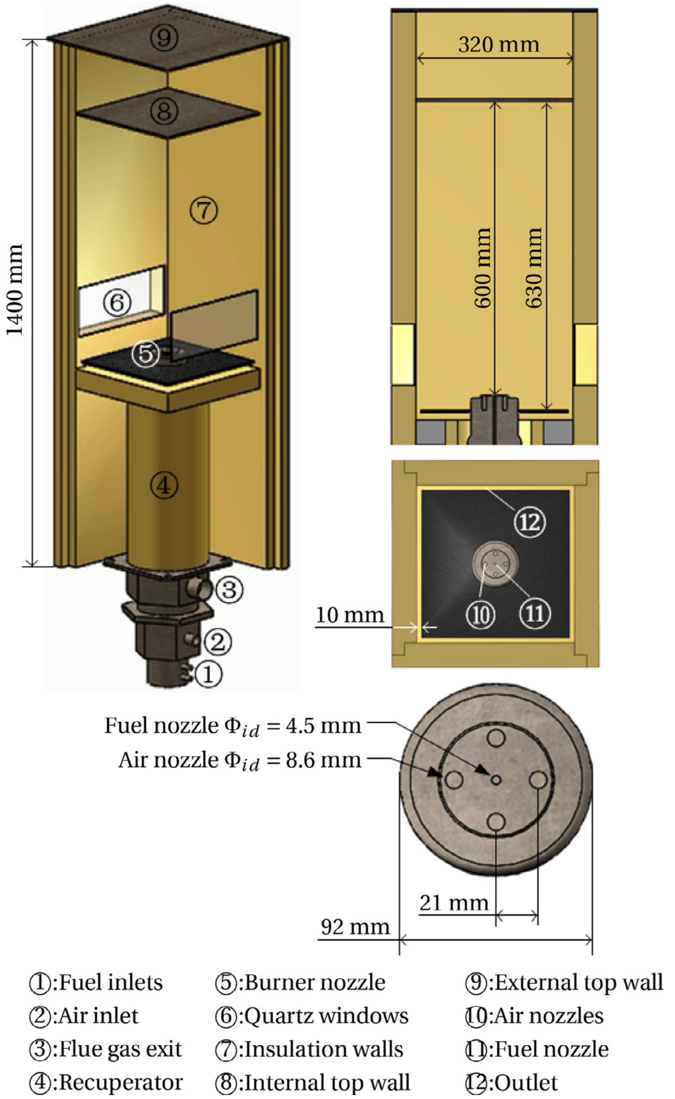

Fig. 3. The schematic of the lab-scale furnace (left), with a vertical cross section of the combustion chamber (top right), a top view (middle right) and a closeup of the burner nozzle (bottom right).

walls and fixed optical setups. The burner nozzle (92 mm in diameter) is protruding 30 mm into the chamber, and the distance from the nozzle tip to the internal top wall is 600 mm. The burner nozzle consists of one central fuel nozzle with an internal diameter of 4.5 mm and four air nozzles (each having an internal diameter of 8.6 mm) symmetrically located around the fuel nozzle. The distance between the fuel nozzle axis and each air nozzle axis is 21 mm. The furnace internal and external top walls are both 310 stainless steel plates, acting as a heat sink and not insulated. This cooling method was chosen because it causes less internal flow complexity than internal cooling tubes. Two opposing side walls are equipped with quartz windows with a size of 280 mm×100 mm to provide optical access for laser diagnostics. To minimize heat loss through the windows, these are covered by ceramic foam apart from a small circular opening where the LDA or CARS laser beams can pass through. A more detailed description can be found in Ref. [2].

Table 1
Composition of Dutch natural gas used in this study.

Species	CH_4	C_2H_6	N_2	CO_2
[mole %]	81.3	3.7	14.4	0.6

Table 2
Settings of the case $\phi = 0.8$. P represents thermal input, ϕ represents equivalence ratio, T_f and T_a are the inlet temperature for fuel and air, $\dot{m}_f$ and $\dot{m}_a$ are mass flow rate for fuel and air, respectively.

P (kW)	ϕ	T_f (K)	T_a (K)	$\dot{m}_f$ (kg/s)	$\dot{m}_a$ (kg/s)
9	0.8	416	816	2.37×10^{-4}	3.87×10^{-3}

3.2. Experimental database

Experiments were done using Dutch natural gas as fuel and at a thermal input of 9 kW (fuel mass flow rate based) at three values of the equivalence ratio ϕ, namely 0.7, 0.8 and 0.9. The case with $\phi = 0.8$ is selected as the validation case for the numerical modelling in this study. The composition of Dutch natural gas is listed in the Table 1. In the simulation, the rest species is represented by CO_2. The detailed settings of the case are summarized in the Table 2. Along several horizontal cross sections the mean axial and radial velocity components and the Reynolds normal and shear stresses were measured using LDA. The mean quantities are averaged from 5000 samples at each measurement point. The one-point of temperature was measured using CARS which was reported by van Veen et al. [32] that the single-shot imprecision of the CARS system is 1–4% over a range from 2000 K to 300 K. Mean temperatures at each point are averaged over 1600 samples in the reaction zone and over 1000 samples out of the reaction zone. Wall temperatures were measured using thermocouples, but the values were not corrected for radiation heat loss. A detailed description of the experimental datasets can be found in Ref. [2].

4. Computational setup

4.1. Computational domain

The computational domain covers the entire volume of the furnace box. Since small round orifices are combined with a large cuboid, a multi-block approach was used to obtain a good quality mesh. An O-grid was used to handle the round orifices. The resultant blocking for the burner nozzles and the corresponding mesh for inlets are shown in Fig. 4. The small blue disc is the fuel inlet and the four red discs are the four air inlets. The five yellow cylindrical surfaces indicates the inlet tubes. The green area indicates the furnace outlet. The grey surfaces indicates the furnace walls.

In zone with merging jets the grid has been refined. At larger distance from the centre cell length in circumferential direction becomes larger. To avoid too large cell aspect ratio, staged refinement in circumferential direction was applied. Two different mesh sizes with 2.5 and 9.5 million hexahedral cells were compared. The coarse mesh gives nearly the same results as the fine one. Therefore, the coarse mesh is used in the following.

4.2. Boundary conditions

The known overall fuel and air flow rates in Table 2 were used to set the mass flow rate at the inlets of fuel and air. In addition, the following boundary conditions at fuel and air inlet were applied.

Fuelinlet	**Air inlet**
$\widetilde{Z} = 1$	$\widetilde{Z} = 0$
$\widetilde{Y_c} = Y_{c,f}$	$\widetilde{Y_c} = 0$
$\widetilde{Y_d} = 0$	$\widetilde{Y_d} = 0$
$\widetilde{h} = h_f$	$\widetilde{h} = h_{air}$

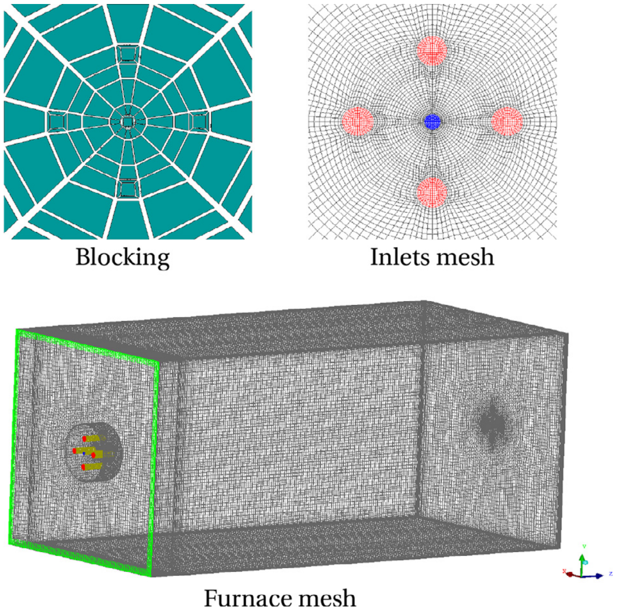

Fig. 4. Illustration of the meshing strategy for furnace inlets.

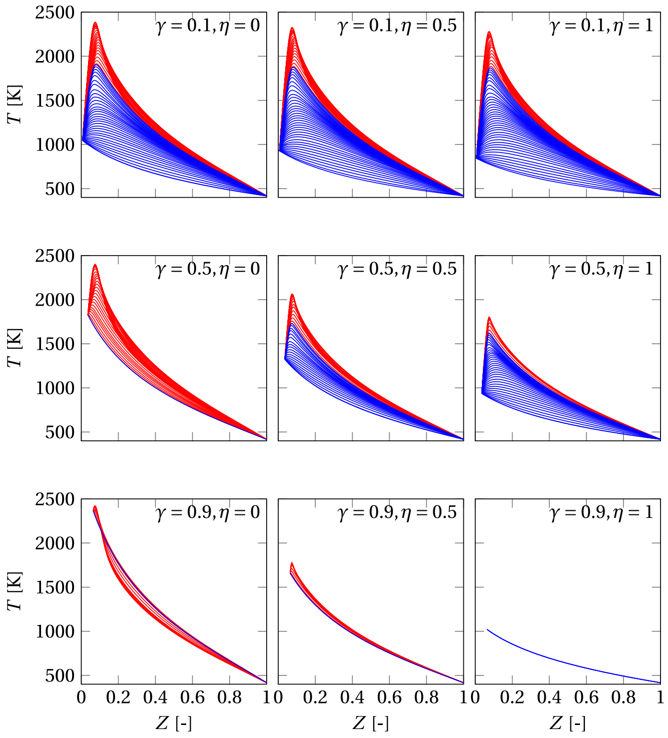

Fig. 5. Temperature profiles in flamelets calculated at different air dilution level γ and enthalpy loss factor η. Red lines represent steady flamelets and blue lines represent an unsteady extinguishing flamelet. (For interpretation of the references to color in this figure legend, the reader is referred to the web version of this article.)

where $Y_{c,f}$ is the value of progress variable computed from the fuel composition, h_f and h_{air} are the enthalpy in fuel and air stream respectively. The variances for mixture fraction and progress variable are both set at zero, $\widetilde{Z''^2} = 0$ and $\widetilde{Y_c''^2} = 0$.

The value of temperature at the side wall at the heights where CARS temperature measurements were made is set to be 60 K lower than the mean temperature measured using CARS at 40 mm away from the wall. The temperature at the side wall at any other height is obtained by linear interpolation or extrapolation between the two nearest values derived from the CARS measurements. The top wall is assumed to have uniform temperature and is set at the temperature at highest position of the side wall. The bottom wall is assumed to be adiabatic. The walls are treated as grey diffusive walls in radiation modelling. The emissivity is 0.8 for all walls. In order to compute the enthalpy at walls based on wall temperatures, a combination of temperature and mixture fraction is needed. In this study, fuel and air can be treated well mixed at walls. Thus, mixture fraction at wall equals to mixture fraction Z_ϕ at global equivalence ratio. Then the enthalpy at the walls is determined assuming chemical equilibrium. Boundary conditions for $\widetilde{Z}$, $\widetilde{Z''^2}$, $\widetilde{Y}_c$, $\widetilde{Y_c''^2}$ and $\widetilde{Y}_d$ are all zero gradient at walls.

4.3. Non-adiabatic DA-FGM library generation

A non-adiabatic DA-FGM library was generated following the theory described in Section 2.1.3. First the boundary conditions for the counterflow flames are defined: pure fuel at the fuel side and pure or diluted air at the oxidizer side. The diluted air composition was calculated by using the TU Delft FLAME code [33] at the mixture fraction $Z = \gamma Z_{st}$ at a specified enthalpy loss.

According to the wall boundary temperature discussed earlier, the maximum enthalpy loss for the considered case is found to be $\Delta h_{\phi,max} = 2.341 \times 10^6$J/kg. Note that this enthalpy loss value is the enthalpy loss in air-diluent mixture. The enthalpy loss in the diluent accordingly equals $\Delta h_{\phi,max}/\gamma$. For a number of dilution levels γ and enthalpy loss Δh, the equilibrium composition is obtained using the TU Delft FLAME code. For the prepared boundary conditions, laminar diffusion counterflow flames are computed in physical space using CHEM1D [34]. The GRImech 3.0 reaction mechanism is used. For selected values of combination of dilution level and enthalpy loss, a two-dimensional FGM is constructed from steady flamelets covering the range of strain rate from a small value until extinction value and an unsteady extinguishing flamelet to cover the low progress variable value range. Next all two-dimensional FGMs are combined to a four-dimensional FGM. The 2D FGM table uses a 51×51 grid in (Z, c)-space, with more finer grid in the range $Z < 0.16$. The 4D FGM table uses a uniformly distributed 11x11 grid in η and γ. Finally the mean quantities are calculated using integration with the PDF of mixture fraction and progress variable. The validation of the accuracy of the tabulation has been reported in [2]. Figure 5 shows some examples of flamelet temperature data generated at air dilution level γ=0.1, 0.5 and 0.9, and enthalpy loss factor η=0, 0.5 and 1. η=0 corresponds to no enthalpy loss in diluent and η=1 represents maximum enthalpy loss in diluent. The corresponding progress variable source terms in each condition are plotted in Figure 6. The flamelets are plotted as temperature versus mixture fraction Z based on fuel and pure air. With diluted air, the starting point of flamelets at the oxidizer side gradually shifts towards the stoichiometric mixture fraction Z_{st} as air dilution level increases to 1.

As mentioned earlier, chemical reactions are affected by products dilution. That is, the progress variable source terms are strongly dependent on the air dilution level. This is illustrated in Fig. 7, where the progress variable source term at different air dilution levels are plotted as a function of Y_c. It clearly shows the impact of heat loss and dilution on the reaction source term. It is seen that the values of reaction source term become smaller and the peak values shift to larger Y_c when air dilution level increases. In addition, the reaction source term at the same air dilution level becomes smaller when enthalpy loss increases.

5. Results and discussions

In the following the results of three simulations are presented and compared, i.e., the full model as explained above, and two

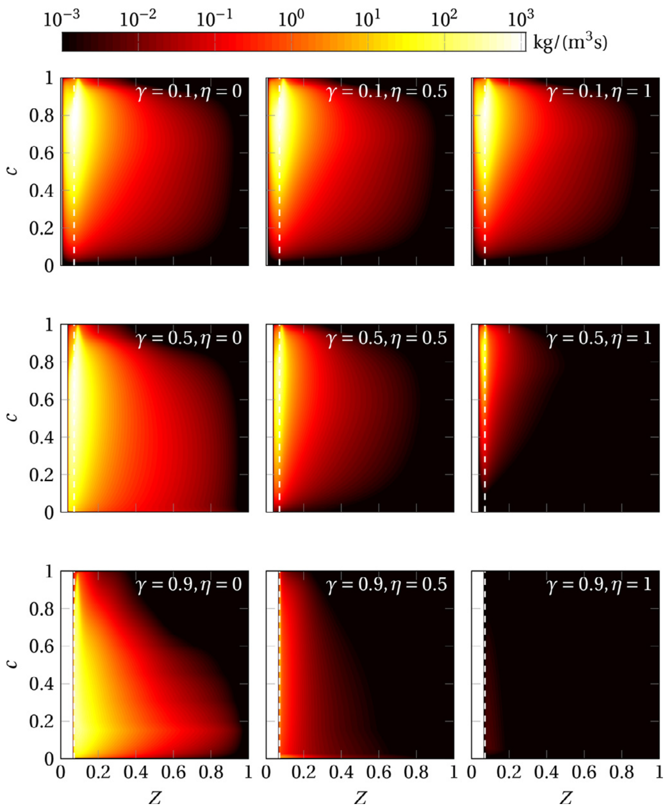

Fig. 6. Progress variable source term in (Z, C) space at different air dilution level γ and enthalpy loss factor η corresponding to the flamelets in Fig. 5. The white dashed line represents the position of stoichiometric mixture fraction for fuel and undiluted air.

simplified models with radiative heat transfer neglected and with radiative heat transfer and progress variable fluctuations neglected. After a discussion of the mean flow patterns the results for velocity and temperature predicted by the full model are compared to the experimental results. Next, mean temperature fields of the full model are compared to those of the simplified models.

5.1. Mixing pattern and MILD combustion

Mixing between fuel, air and burnt gases is a key factor in MILD combustion. A first view on this mixing process is provided by the mean flow patterns. Figure 8 shows the mean flow pattern in the mid plane (parallel to two side walls and crossing the fuel jet and two air jets) and the diagonal plane (from corner to corner, crossing the fuel jet and passing in between neighbouring air jets). The white curves shows the mean flow direction and the red cures

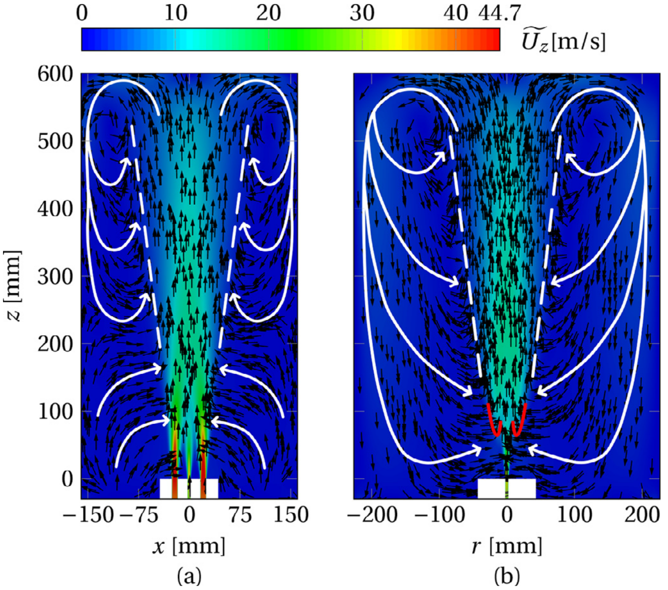

Fig. 8. Predicted mean flow field in the furnace. (a): middle plane across fuel and two air jets; (b): diagonal plane, r is the Euclidean distance to fuel nozzle centre.

show the boundary where adjacent air jets start interacting with each other. The flow patterns are different in these two planes. In the mid plane, there are two recirculation zones in the upper part of the furnace as illustrated by the white solid lines. In the diagonal plane, the recirculation zones span nearly the entire height of the furnace showing that burnt gases mainly flow down in the corner regions, along the four vertical edges of the combustion chamber. Below the lowest positions indicated by the red curves, the four air jets and the fuel jet develop independently and are diluted directly by entrained burnt gases. Above this position, the fuel jet is totally surrounded by air jets which blocks the direct entrained burnt gases by the fuel jet. Here, further dilution can only be achieved by turbulent mixing transporting burnt gases from the air jets outer boundaries to the inner region. The first (lower) and second (upper) stages of the fuel jet dilution will be called direct and indirect dilution stage, respectively. Indeed, there are two essential factors to establish MILD combustion using this burner nozzle configuration. The first is a sufficiently high turbulence level which prevents the formation of an attached flame. The second is dilution achieved by internal recirculation driven by the jets. The amount of burnt gases entrained by the jet flows depends on the jets momentum and the air jets arrangement determining the height where the direct dilution stage ends. For larger distance between fuel and air jets, this height becomes larger providing more optimal conditions for direct dilution. However, when the distance between the fuel jet and the air jets becomes too high, the reac-

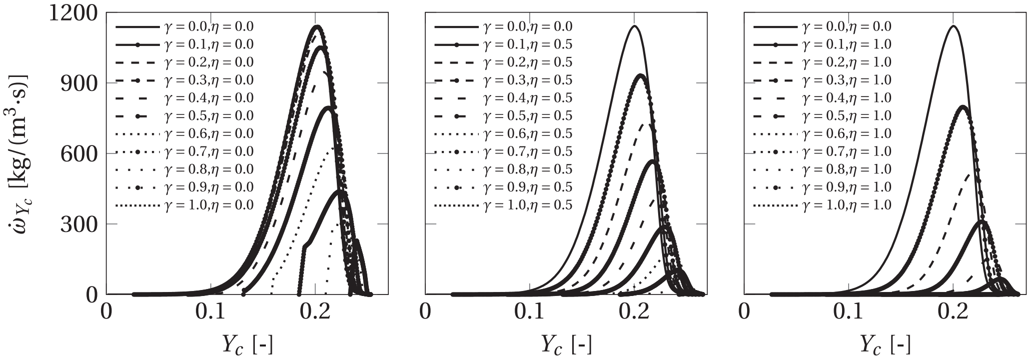

Fig. 7. Variations of progress variable source term at enthalpy loss factor η=0, 0.5 and 1 are plotted as a function of Y_c at different air dilution levels. .

tion zone is no longer clearly coupled to the jet mixing zone and incomplete combustion might become an issue in a large furnace space.

5.2. Velocity prediction

Next we discuss the comparison between measured and computed velocity statistics. Before making the comparison, the experimental radial profiles at z=100 mm to z=500 mm are slightly shifted to impose the expected symmetry with respect to the centerline. The deviation from this symmetry is attributed to a slight asymmetry in the supply lines of air to the burner. The measured mean vertical velocity $\widetilde{U}_z$ is shifted by a distance z·tanθ in the negative x-direction. The angle θ is such that the shear stress satisfies $\widetilde{u_z''u_x''} = 0$ on the centerline. This is realised by taking tan$\theta \approx 0.03$. The measured mean radial velocity $\widetilde{U}_x$ is shifted by a constant value of -0.3 m/s to make $\widetilde{U}_x = 0$ on the centerline and also the experimental profiles of turbulent kinetic energy and the mean and the variance of temperature are shifted in the same way.

Figure 9 shows the comparison between the predicted mean velocity (solid lines) and the measured mean velocity (symbols). At the nozzle exit (z=3 mm), the agreement for mean vertical velocity $\widetilde{U}_z$ is excellent. The peak mean velocity is over predicted at z=50 mm and z=100 mm. At higher positions from z=200 mm to z=500 mm, the overall agreement is quite good. For the mean velocity in radial direction $\widetilde{U}_x$, the overall trends are captured and the positions of the peaks on the profiles are also well captured. However, the local extreme values on the profiles at z=50 mm and z=100 mm are not well-predicted.

Figure 10 displays the results for the turbulence kinetic energy. It is seen that the turbulence kinetic energy is under predicted at height z=50 mm, and over predicted at z=100 mm and z=200 mm. Satisfactory predictions are obtained at z=300 mm and z=400 mm. But the discrepancies between experiment and prediction become larger again at z=500 mm. The good level of agreement observed for velocity statistics (mean and TKE) is due to the combined effect of turbulence model, combustion model and radiation model and their couplings. The results for the velocity statistics obtained here using DA-FGM in general are of similar quality as the results obtained using EDC models and FGM with pure fuel and pure air flamelets in Ref [9] (Figure 6 and dummyTXdummy-(Figure 7), but results obtained using DA-FGM are better at z=500 mm.

5.3. Temperature prediction

A comparison between the predicted and the measured mean temperature is shown in Fig. 11. Near the nozzle exit, at z=25 mm, the mean temperature is very well predicted, but it is somewhat under predicted in the central region from z=100 mm to z=300 mm. This can be connected to the under prediction of the turbulence kinetic energy. In the region below z=100 mm the turbulent mixing rate is under estimated. In that case, the mixing with burnt gases is under predicted explaining the lower mean temperature. The turbulent kinetic energy is over predicted at z=100 mm and z=200 mm. The associated high turbulent mixing rate can provide an explanation why the predicted mean temperature is getting closer to the measured mean temperature from z=200 mm to z=300 mm. Further downstream, the difference between predicted and measured mean temperatures become smaller. The mean temperature increase from z=400 mm to z=500 mm is due to combustion and is well-predicted. The maximum mean temperature increase between z=400 mm and z=500 mm is about 135 K, and the predicted overall mean temperature increase from air temperature to burnt state is less than 615 K. This good level of agreement is obtained only when both radiation and progress variable fluctuations are included in the model as discussed in the next subsection.

The results for the mean temperature obtained here using DA-FGM are in general very close to the results using the NE-EDC model presented in Ref [9], (Figure 5). This illustrates that models based on different concepts, flamelet based and stirred-reactor based can deliver equally good results. But in contrast with NE-EDC, the DA-FGM also can provide predictions of variances and other statistical properties. The predicted temperature root mean square is compared with measured temperature RMS in Fig. 12. It is seen that the predicted temperature RMS agrees with the measured values but some systematic deviations are observed. In the non-reacting region or recirculation region, the measured temperature RMS is at a level of about 80 K, and the predictions are systematically 30 to 50 K lower. The cause is not fully clear but may be related to the unavoidable RMS coming from the experimental error. At higher positions where reactions take place, the predicted temperature RMS in the reaction zone are in good agreement with experimental data. This shows that the DA-FGM provides good capability to predict the scalar variances produced by reactions. More accurate prediction of scalar variances can be obtained by using LES.

Figure 13 presents profiles of the temperature, the dilution level α and the air dilution level γ along the central axis. The mean temperature profile along the line may be divided into three regions. The first region is below z=100 mm and corresponds to the direct dilution stage. The second region is from z=100 mm to z=400 mm and corresponds to the indirect dilution phase. The third region is the combustion stage. The first region can be divided into two sub-regions. Below z=50 mm, the fuel is mixing with burnt gases, the air dilution level γ is flat and the mean temperature along the centreline increases very fast. Above z=50 mm, the centreline region starts being slightly influenced by the air stream. The mean temperature rise slows down slightly. This is indicated by the decrease in the air dilution level from z=50 mm to z=100 mm. The diluent mass fraction α is still increasing, but it reaches a peak at z≈100 mm. The diluent is coming from the direct entrainment by the jets near the nozzle exit. It is seen from the air dilution level profile that air starts affecting the centreline region from z=50 mm onward. The air jets shear layers bring more diluent to the centreline region. This explains why the diluent mass fraction is still increasing. However, as air jets develop, the jets inner part (which is much less diluted) start affecting the centreline region, the dilution level accordingly decreases, and temperature rise becomes very slow due to the lower air temperature. That is, the indirect dilution phase starts. Further downstream, more diluent from the recirculation region is transported into the central region by turbulent mixing, thus the dilution level starts increasing again. Above z=400 mm the mean temperature rises more rapidly with height due to the heat release from reactions. This prediction is consistent with the position of the reaction zone indicated by experimentally observed OH* chemiluminescence (Fig. 13). However, it should be noted that the OH* image is an integration of the OH* chemiluminescence signal from the view direction of the camera. Its intensity does not relate to the magnitude of heat release rate.

5.4. Influence of radiation and progress variable fluctuation

The question arises how important it is to include the influence of radiative heat transfer and the influence of progress variable fluctuations in the model. This becomes clear from Fig. 14. It shows the result of simulations (a) excluding radiation and progress variable fluctuations, (b) including radiative heat transfer but excluding progress variable fluctuations and (c) results including radiation and progress variable fluctuations. The predicted mean tem-

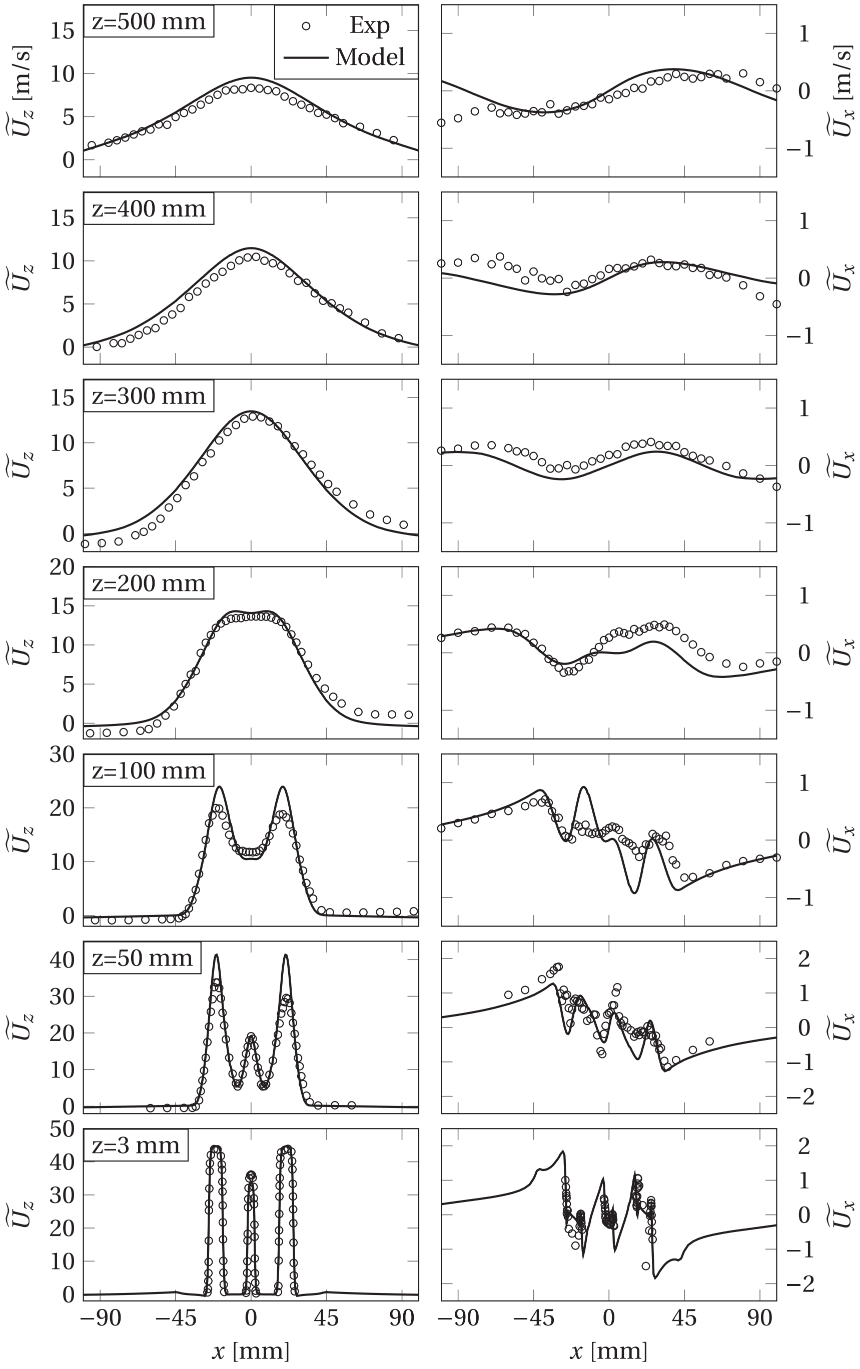

Fig. 9. Comparison between the predicted and the measured mean axial velocity component (left) and the mean radial velocity component (right).

perature fields are quite different. Without progress variable fluctuations taken into account, the peak mean temperature in the reaction zone is 1900 K without radiation, and 1677 K with radiation. Without radiation, a significant mean temperature increase occurs very early, i.e., below z=100 mm, and reactions are taking place already in the mixing layers between the jets. With radiation included, the high temperature zone is shifted to above z=300 mm. The radiation heat loss lowers the mean temperature of the recirculated products slowing down the reaction progress and also leading to a steady state at lower mean temperature. The predicted mean temperature field is also influenced by the treatment of progress variable fluctuations. Figure 14(b) and (c) shows the results of simulations including radiation and respectively excluding and including progress variable fluctuations. The predicted peak mean temperature in the furnace is reduced to 1430 K when progress variable fluctuations are taken into account by a presumed β-PDF. This result shows that the assumed PDF model describes an essential aspect of the non-homogeneous burning also observed in the chemiluminescence and CARS experimental data. Taking these fluctuations into account the homogeneous mean temperature in the furnace is accurately predicted as already shown in the detailed comparison between predicted and measured mean temperature in Section 5.3.

Figures 15 and 16 show the predicted mean fields of $\widetilde{Z}$, $\widetilde{Y_c}$, $\widetilde{Y_d}$, $\widetilde{Z''^2}$, $\widetilde{Y_c''^2}$ and $\widetilde{h}$ in the case where both radiation and progress variable fluctuation are included. The difference between $\widetilde{Y_c}$ and $\widetilde{Y_d}$ in the range between z=400 mm and z=600 mm is quite clear, as shown in Fig. 15. The increase of dilution variable is delayed com-

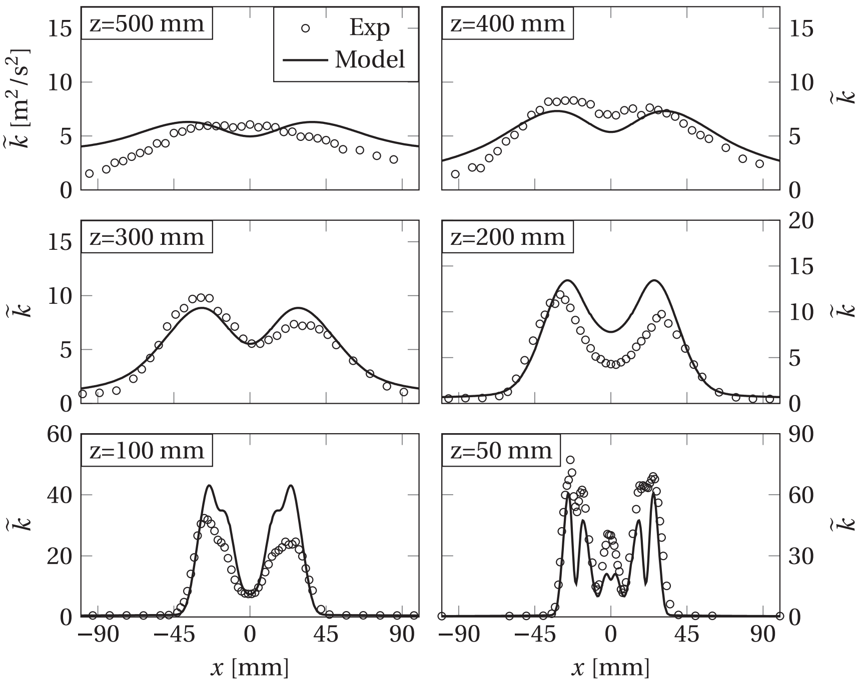

Fig. 10. Comparison between predicted mean and measured turbulence kinetic energy.

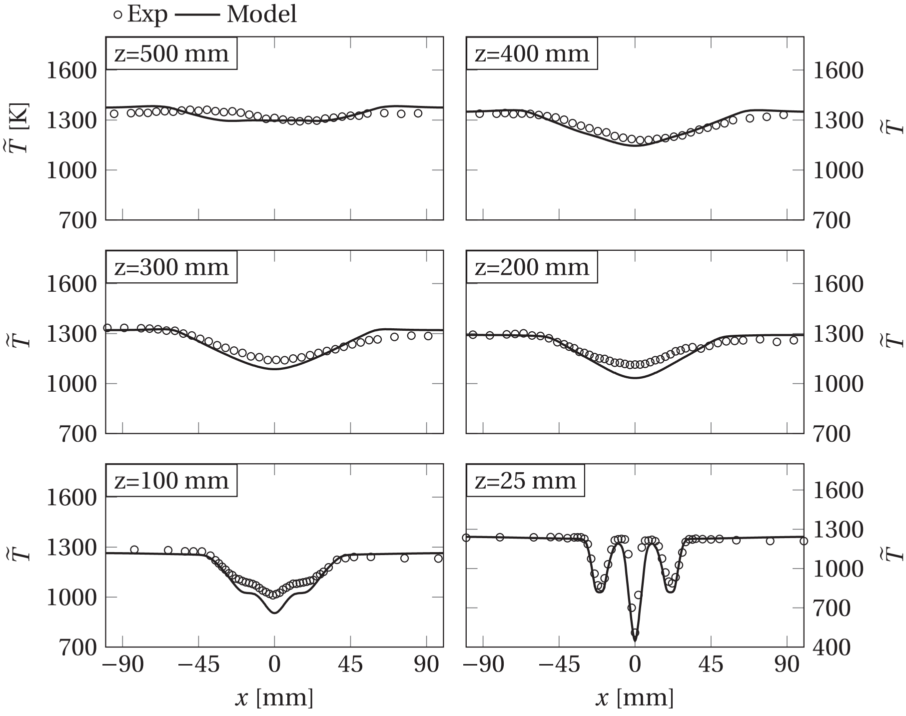

Fig. 11. Comparison between predicted and measured mean temperature.

pared to progress variable, and this is in full agreement with the method for dilution stream modelling. Progress variable increases as reaction is progressing, and when complete reaction is reached, dilution variable starts to increase.

Figure 17 shows contour plots of the progress variable source term with and without the effect of dilution. The contour plot without dilution effect is obtained from post-processing by setting $Y_d = 0$. By definition of the DA-FGM model, setting $Y_d = 0$ corresponds to absence of dilution but also vanishing heat loss. Both effects influence the difference between the contour plots in Fig. 17. The high values obtained when setting $Y_d = 0$ express the combined effect of absence of dilution and absence of heat loss. Displaying the effect of only absence of dilution and keeping heat loss is not possible with the DA-FGM tables. But it is clear that a reaction zone distributed over a large volume, as present in the MILD combustion regime, is obtained only when using diluted flamelets. When the dilution effect is not included, reaction progress is very rapid close to the burner leading to a narrow reaction zone, not in agreement with experiments. Figure 18 shows the scatter plots of values of source term values versus Z_0 and C. According to the

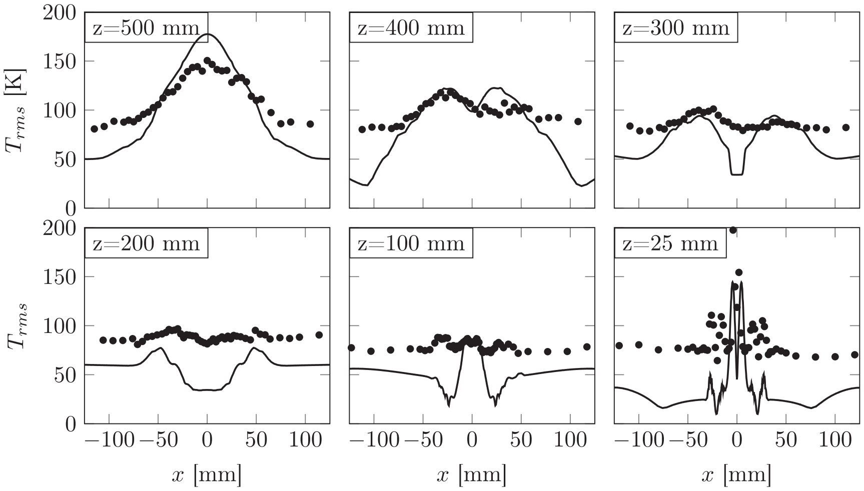

Fig. 12. Comparison of measured temperature RMS (black dots) and predicted temperature RMS T_{rms} (solid line) at different heights.

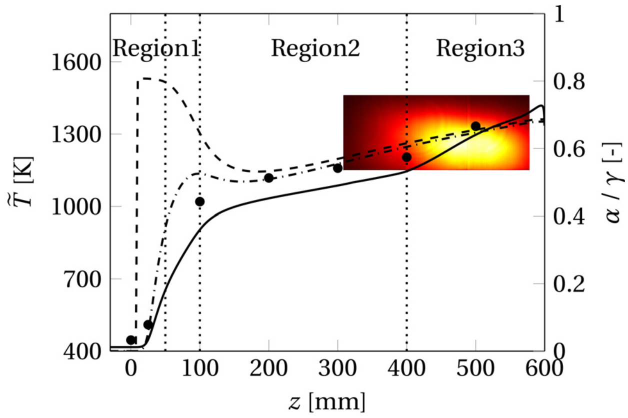

Fig. 13. Profiles of the predicted mean temperature $\widetilde{T}$ (solid line), air dilution level γ (dashed line) and dilution level α (dash-dotted line) along the central axis. The black dots are measured mean temperature. The inset represents the experimental observed OH* chemiluminescence.

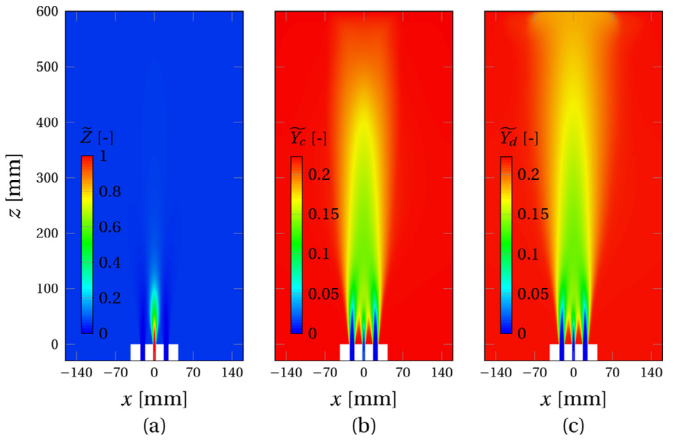

Fig. 15. Predicted mean scalar fields in the furnace. (a): mean mixture fraction; (b): mean progress variable, (c): mean dilution variable.

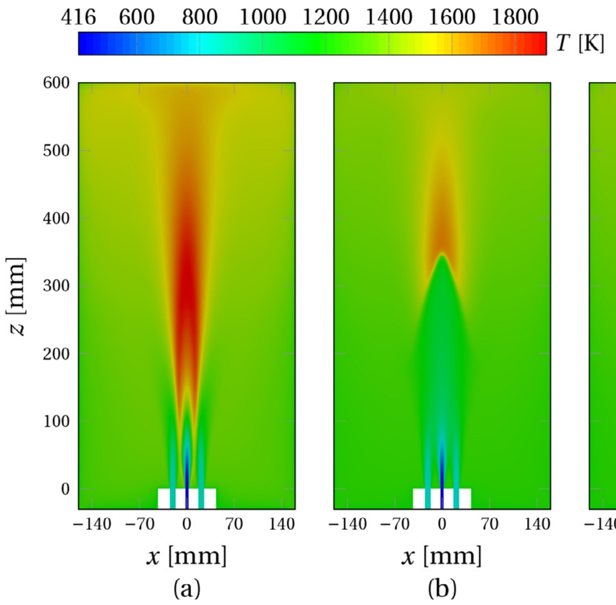

Fig. 14. Predicted mean temperature fields on the cross section through the midplane: (a) excluding radiation and progress variable variance, (b) including radiation and excluding progress variable variance, (c) including radiation and progress variable variance.

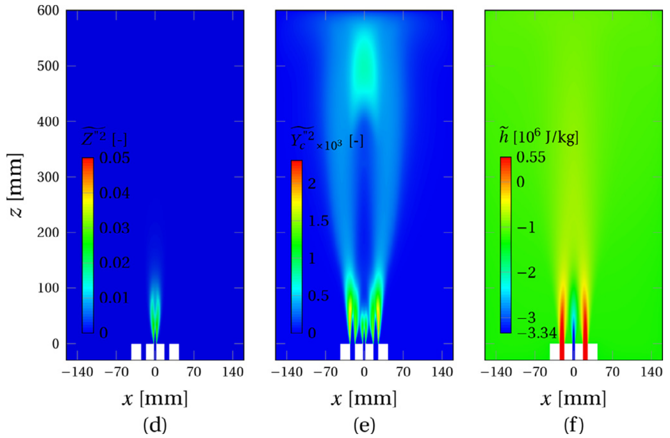

Fig. 16. Predicted mean scalar fields in the furnace. (a): mean mixture fraction variance; (b): mean progress variable variance, (c): mean enthalpy.

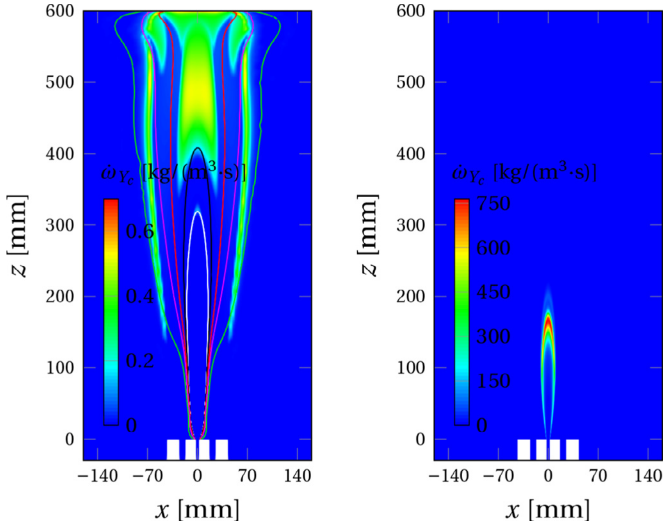

Fig. 17. Comparison of progress variable source term contour plot between the results predicted by DA-FGM (left) and the results using undiluted flamelets (i.e. setting $Y_d = 0$ in post-processing) (right). The contour lines in the left plot indicate Z_0 at 0.005 (green), 0.018 (purple), 0.028 (red), 0.043 (black) and 0.054 (white). (For interpretation of the references to color in this figure legend, the reader is referred to the web version of this article.)

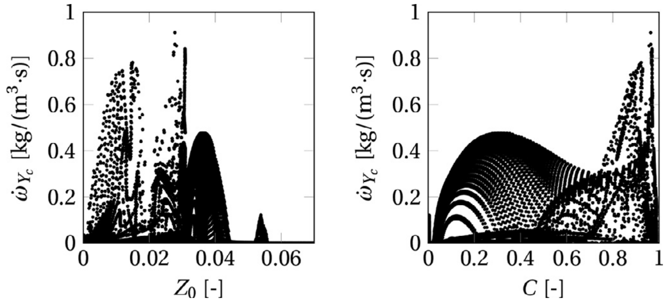

Fig. 18. Progress variable source term scatter plot over Z_0 and C. .

scatter plot of source term over Z_0, reactions mainly take place at lean condition over Z from 0 to 0.043. The top of the main reaction zone is impinging on the top wall as can be seen from the reaction zone shape. The two stripe-like reaction zones are typical diffusion flames, oriented parallel to equal mean mixture fraction contours. Different zones in the scatter plots are associated with different zones in the furnace. A first region in the scatter plots ranges over $Z_0 = 0 \sim 0.18$ and $C = 0 \sim 1$. It corresponds to the diffusion flame zone. A second one ranges over $Z_0 = 0.18 \sim 0.28$ and $C = 0.7 \sim 1$. This is related to the impinging reaction zone. The third one is the main reaction zone ranging over $Z_0 = 0.28 \sim 0.43$ and $C = 0 \sim 0.7$. The small peak around $Z_0 = 0.54$ in the first scatter plot corresponds to the small peak at nearly zero value of C in the second scatter plot. Because it has negligible impact on the simulation results we have not further investigated the cause of this small peak, but presumably it is a numerical artefact.

Using the observations on progress variable source term, we can now give further explanation of the contour plot of $\widetilde{Y_c''^2}$ in Fig. 16. The fluctuations of Y_c can be caused by fluctuations in reaction progress and by fluctuations in mixture fraction. In the main reaction zone they are mainly due to reactions. On the other hand the fluctuations below z=150 mm are in the jets shear layers and more caused by mixture fraction fluctuations. Fluctuations in diffusion flame zones are caused by both mixing and reaction. In the regions where reactions take place, the dilution level is above 0.6. This leads to small difference between the minimal and maximal values of unscaled progress variable, Y_c^b and Y_c^u. Nevertheless the progress variable fluctuations (See Fig. 16) are important to obtain the mean temperature and temperature standard deviation in the upper region of the furnace in agreement with the experimental results.

5.5. Importance of spectral modelling and turbulence radiation interaction

The simulations reported above have used a grey absorption coefficient obtained from a WSSG model. This method is widely used in furnace simulations in the literature, but is known to provide inaccurate results. On the other hand the calculation has included the influence of turbulence radiation interaction, which is often neglected in furnace simulations in the literature. To provide more insight in the relative importance of spectral modelling and TRI, we here present a simple sensitivity analysis. Rather than repeating the complete CFD simulation with spectral radiative transfer, the sensitivity is checked by calculating in four different ways the evolution of radiative intensity under the influence of emission and absorption along horizontal lines at the heights where experimental data on temperature statistics are available. Selecting from grey radiative transfer or spectral radiative transfer, without or with TRI, four ways of calculation have been applied.

According to the WSGG model, the total emissivity associated with transfer in a gas of uniform composition and temperature over a length L is given by

$$\varepsilon = \sum_{j=0}^{J} a_j(T)\left[1 - \exp\left(-\kappa_j L(X_{CO_2} + X_{H_2O})\right)\right] \qquad (45)$$

where the absorption coefficient κ_j has units $1/m$. The grey treatment of radiative heat transfer makes use of an effective absorption coefficient obtained from a mean beam length and was used to obtain the results presented in previous sections. In the more accurate spectral simulation, the transfer is calculated per band. Here results of both methods are compared using the WSGG model of Johansson et al. [26]. In that model $J = 4$ and the coefficients κ_j only depend on the molar ratio of CO_2 to H_2O and the coefficients a_j are in addition temperature dependent. The details are reported in Section 2 of Ref. [26].

The lines along which the evolution of intensity is calculated start close to one sidewall and end close to the opposite wall. At height 25 mm the line traverses zones with low amount of radiative species when crossing the zones dominated by fuel and air jets. At higher height the influence of the jets disappears and the composition becomes more and more uniform, but a zone with

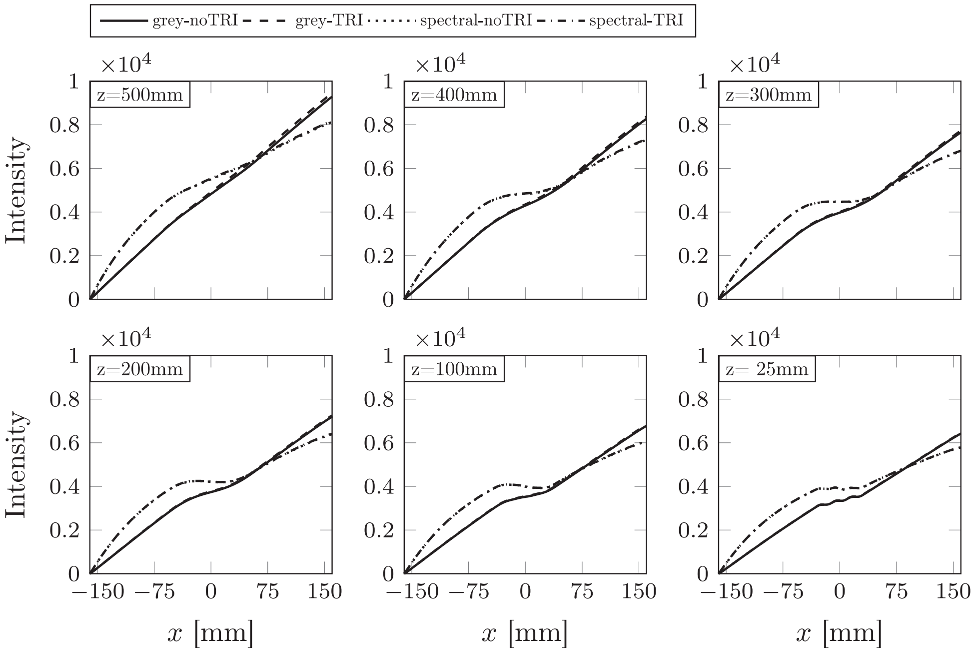

Fig. 19. Intensity evolution along different horizontal traverses.

lower mean temperature is present in the middle. The higher in the furnace, the higher the level of temperature fluctuations in the centre of the furnace. Therefore the line at lower height serves as a test for changes in composition and temperature and the lines at higher height serves as test for the influence of TRI. By comparing the prediction with spectral transfer and TRI included with other predictions with simplification of spectral treatment or neglect of TRI, or both, their relative importance can be judged.

In the following the index n refers to positions along the line, $(y_n - y_{n-1})$ is the length of the segment from position y_{n-1} to position y_n and X denotes mole fraction. When the segments are small enough to assume uniform composition over the length of the segment, the transmissivity in band j is given by

$$\tau_{j,n-1/2} = \exp\left(-\kappa_j \Delta s (X_{CO_2} + X_{H_2O})\right) \tag{46}$$

The evolution of intensity along the considered lines is given by

$$I_{j,n} = I_{j,n-1}\tau_{j,n-1/2} + a_j I_{b_{n-1/2}}\left[1 - \tau_{j,n-1/2}\right] \tag{47}$$

The total intensity at any position can be obtained by summing the intensities in all bands including the clear band at that position.

After Reynolds averaging, the radiative transfer in the j-th band of the spectral model in spatial segment $(n-1, n)$ is given by

$$\bar{I}_{j,n} = \overline{I_{j,n-1}\tau_{j,n-1/2}} + \overline{a_j I_{b,n-1/2}\left[1 - \tau_{j,n-1/2}\right]} \tag{48}$$

Making the usual assumption that local intensity is statistically independent of transmissivity from neighbouring regions (also made in the rest of this article), this equation takes the form

$$\bar{I}_{j,n} = \bar{I}_{j,n-1}\overline{\tau_{j,n-1/2}} + \overline{a_j I_{b,n-1/2}} - \overline{a_j I_{b,n-1/2}\tau_{j,n-1/2}} \tag{49}$$

The mean transmissivity in band j is given by

$$\overline{\tau_j} = \overline{\exp\left(-\kappa_j \Delta s (X_{CO_2} + X_{H_2O})\right)} \tag{50}$$

The turbulent fluctuations in mole fraction of CO_2 and H_2O are of minor impact and in the following only the fluctuations in temperature will be taken into account. To calculate the average $\overline{a_j I_{b,n-1/2}}$ appearing in Eq. (49), we need the averages of powers of T up to order six, because a_j is a second order polynomial of T. These averages have been computed using the PDF of mixture fraction and progress variable. It should be mentioned that the maximum difference between the computed level of fluctuations as expressed by T_{rms} and experimental data is at most 10 K deviation on a value of 160 K. The result of a simulation without TRI can be simply obtained by using the power of the mean of T instead of the mean of powers of T.

The results obtained for the spatial profile of total intensity along the six considered horizontal traverses is shown in Fig. 19. For each traverse the initial value was set as zero in order to focus on the contribution from the gas absorption and emission. The results were checked for dependence on step size Δs and were found almost indistinguishable between step size 0.32 mm and 10 mm. The latter value is within the declared range of validity of the WSGG correlation used. In all four model combinations, differences develop when the beam traverses a region with different temperatures. The profile with the grey models ends at a higher value than the spectral models (corresponding to higher radiative flux). The calculation reveals the influence of TRI and of the spectral modelling of the gas radiative properties on the predicted total intensity arriving at the boundary of the gas cloud. TRI does not make large difference because the level of temperature fluctuations is much small in the flameless combustion regime. Detailed study of TRI can be done by using the methods proposed in Ref. [35]. The difference in predictions of spectral model and grey model at the end of the horizontal traverses are found to be between 11% and 16%. (This calculation is based on the results of spectral model.) This does mean that the full grey CFD simulation has the same error because the simple calculation along horizontal traverses is not including consistency between intensity gradient and energy equation source term. The error of the CFD simulation using grey absorption coefficient can only be quantified by making the full spectral CFD simulation. However, including all radiation related mean quantities in the frame of the tabulated chemistry leads to rather large lookup tables that we currently cannot handle. A large memory per processor is required because for the spectral simulation more variables have to be included in the DA-FGM table (all averages needed in the Reynolds averaged RTE's for all bands) leading to much larger lookup tables than for the grey model. It can be concluded that a simulation along selected lines is very revealing since it shows the systematic deviations at length scales either smaller or larger than the chosen mean beam length. The total intensity along a path predicted using the mean beam length based grey absorption coefficient is too low for path lengths smaller than the mean beam length and too large for path lengths larger than the mean beam length. In a homogeneous medium this directly follows from the different growth rate of emissivity in different bands. Also in the slightly inhomogeneous medium considered here the effect is pronounced.

6. Summary and conclusions

In this study, the DA-GFM model was proposed to account for dilution effects on the reactions in MILD combustion modelling. This chemistry tabulation method includes dilution and enthalpy loss effects on local flame structure. The resulting DA-FGM library consists of a series of flamelets calculated between fuel and pure or diluted air with non-adiabatic effects included. The tabulated chemistry was integrated in a RANS approach for turbulent combustion modelling, including a radiation model and a turbulence-radiation interaction consideration.

The model was validated by an application to MILD combustion in a lab-scale furnace burning Dutch natural gas at power 9 kW and equivalence ratio 0.8. Overall, the simulation results obtained with the proposed models are in very good agreement with experiments. Some sensitivity analysis was performed. Radiative transfer plays an essential role in establishing flame structure. The relative importance of including TRI and spectral treatment of radiation was illustrated by solving the RTE along horizontal traverses. Spectral treatment was found to be more important than TRI and is recommended for further CFD studies of the furnace. Including progress variable fluctuations in addition to the fluctuations of mixture fraction is necessary to obtain good temperature predictions.

The injection strategy influence the mixing processes in the near burner region. Based on the analysis of the flow field, it is found that the distance between fuel and air jets determines the relative importance of the direct dilution phase and the indirect dilution phase. The direct dilution phase occurs before air jets interact with each other, and all jets are diluted independently by entrainment of burnt gases. The indirect dilution phase occurs when air jets are already interacting with each other and is dominated by turbulent mixing, transporting burnt gases from recirculation zone to inner region of the jets. Good predictions for mixing and dilution process before combustion takes place is important because they provide the initial state for combustion. The standard $k-\epsilon$ model in combination of standard gradient diffusion based models for scalar transport were found to perform well.

Declaration of Competing Interest

The authors declare that they have no known competing financial interests or personal relationships that could have appeared to influence the work reported in this paper.

Acknowledgments

The authors would like to thank the China Scholarship Council (CSC) for financial support for the first author. The authors acknowledge funding by Technology Foundation STW for the construction of the furnace. This work was sponsored by NWO Physical Sciences for the use of HPC resources.

References

[1] Y. Minamoto, N. Swaminatham, Modelling paradigms for MILD combustion, Int. J. Adv. Eng. Sci. Appl. Math. 6 (1–2) (2014) 65–75.

[2] X. Huang, Measurements and model development for flameless combustion in a lab-scale furnace, 2018 Ph.D. thesis.

[3] A. Perpignan, A. Gangoli Rao, D. Roekaerts, Flameless combustion and its potential towards gas turbines, Prog. Energy Combust. Sci. 69 (2018) 28–62.

[4] M. Graça, A. Duarte, P.J. Coelho, M. Costa, Numerical simulation of a reversed flow small-scale combustor, Fuel Process. Technol. 107 (2013) 126–137.

[5] A. Rebola, P.J. Coelho, M. Costa, Assessment of the performance of several turbulence and combustion models in the numerical simulation of a flameless combustor, Combust. Sci. Technol. 185 (4) (2013) 600–626.

[6] D. Lupant, P. Lybaert, Assessment of the EDC combustion model in MILD conditions with in-furnace experimental data, Appl. Therm. Eng. 75 (2015) 93–102.

[7] V. Fortunato, C. Galletti, L. Tognotti, A. Parente, Influence of modelling and scenario uncertainties on the numerical simulation of a semi-industrial flameless furnace, Appl. Therm. Eng. 76 (2015) 324–334.

[8] A. Parente, M.R. Malik, F. Contino, A. Cuoci, B.B. Dally, Extension of the eddy dissipation concept for turbulence/chemistry interactions to MILD combustion, Fuel 163 (2016) 98–111.

[9] N. Romero-Anton, X. Huang, H. Bao, K. Martin-Eskudero, E. Salazar-Herran, D. Roekaerts, New extended eddy dissipation concept model for flameless combustion in furnaces, Combust. Flame 220 (2020) 49–62.

[10] X. Huang, M.J. Tummers, D.J.E.M. Roekaerts, Experimental and numerical study of MILD combustion in a lab-scale furnace, Energy Proc. 120 (2017) 395–402.

[11] E. Abtahizadeh, J. van Oijen, P. de Goey, Numerical study of MILD combustion with entrainment of burned gas into oxidizer and/or fuel streams, Combust. Flame 159 (6) (2012) 2155–2165.

[12] C. Locci, O. Colin, J.-B. Michel, Large eddy simulations of a small-scale flameless combustor by means of diluted homogeneous reactors, Flow, Turbul. Combust. 93 (2) (2014) 305–347.

[13] C. Locci, O. Colin, D. Poitou, F. Mauss, A tabulated, flamelet based NO model for large eddy simulations of non-premixed turbulent jets with enthalpy loss, Flow, Turbul. Combust. 94 (4) (2015) 691–729.

[14] J. Lamouroux, M. Ihme, B. Fiorina, O. Gicquel, Tabulated chemistry approach for diluted combustion regimes with internal recirculation and heat losses, Combust. Flame 161 (8) (2014) 2120–2136.

[15] O. Colin, J.-B. Michel, A two-dimensional tabulated flamelet combustion model for furnace applications, Flow, Turbul. Combust. 97 (2) (2016) 631–662.

[16] A.S. Veríssimo, A.M.A. Rocha, M. Costa, Operational, combustion, and emission characteristics of a small-scale combustor, Energy Fuels 25 (6) (2011) 2469–2480.

[17] G. Sorrentino, P. Sabia, M. de Joannon, A. Cavaliere, R. Ragucci, The effect of diluent on the sustainability of MILD combustion in a cyclonic burner, Flow, Turbul. Combust. 96 (2) (2016) 449–468.

[18] Z.X. Chen, N.A.K. Doan, X.J. Lv, N. Swaminathan, G. Ceriello, G. Sorrentino, A. Cavaliere, Numerical study of a cyclonic combustor under moderate or intense low-oxygen dilution conditions using non-adiabatic tabulated chemistry, Energy Fuels 32 (10) (2018) 10256–10265.

[19] G. Ceriello, G. Sorrentino, A. Cavaliere, P. Sabia, M. de Joannon, R. Ragucci, The role of dilution level and canonical configuration in the modeling of MILD combustion systems with internal recirculation, Fuel 264 (2020) 116840.

[20] P.J. Coelho, Turbulence-radiation interaction: from theory to application in numerical simulations, J. Heat Transf. 134 (3) (2012) 1–13.

[21] G. Li, M.F. Modest, Importance of turbulence-radiation interactions in turbulent diffusion jet flames, J. Heat Transf. 125 (5) (2003) 831–838.

[22] A. Habibi, B. Merci, D. Roekaerts, Turbulence radiation interaction in reynolds-Averaged navier-Stokes simulations of nonpremixed piloted turbulent laboratory-scale flames, Combust. Flame 151 (1–2) (2007) 303–320.

[23] T. Poinsot, D. Veynante, Theoretical and numerical combustion, Third, Aquaprint, 2012.

[24] B.A. Albrecht, S. Zahirovic, R.J.M. Bastiaans, J.A. van Oijen, L.P.H. de Goey, A premixed flamelet-PDF model for biomass combustion in a grate furnace, Energy Fuels 22 (3) (2008) 1570–1580.

[25] J.A. van Oijen, A. Donini, R.J.M. Bastiaans, J.H.M. ten Thije Boonkkamp, L.P.H. de Goey, State-of-the-art in premixed combustion modeling using flamelet generated manifolds, Prog. Energy Combust. Sci. 57 (2016) 30–74.

[26] R. Johansson, B. Leckner, K. Andersson, F. Johnsson, Account for variations in the h_2o to CO_2 molar ratio when modelling gaseous radiative heat transfer with the weighted-sum-of-grey-gases model, Combust. Flame 158 (5) (2011) 893–901.

[27] E.R.G. Eckert, Radiative transfer, h. c. hottel and a. f. sarofim, mcgraw-hill book company, new york, 1967. 52 pages, AIChE J. 15 (5) (2004) 794–796.

[28] M.F. Modest, Radiative heat transfer, Second, McGraw-Hill, New York, 2003.

[29] W.A. Fiveland, Discrete-ordinates solutions of the radiative transport equation for rectangular enclosures, ASME Trans. J. Heat Transf. 106 (1984) 699–706.

[30] P.J. Coelho, Numerical simulation of the interaction between turbulence and radiation in reactive flows, Prog. Energy Combust. Sci. 33 (4) (2007) 311–383.

[31] V.P. Kabashnikov, G.I. Kmit, Influence of turbulent fluctuations on thermal radiation, J. Appl. Spectrosc. 31 (2) (1979) 963–967.

[32] E.H. van Veen, D. Roekaerts, Thermometry for turbulent flames by coherent anti-stokes raman spectroscopy with simultaneous referencing to the modeless excitation profile, Appl. Opt. 44 (32) (2005) 6995–7004.

[33] T.W.J. Peeters, Numerical modeling of turbulent natural-gas diffusion flames, 1995 Ph.D. thesis.

[34] CHEM1D, A one-dimensional laminar flame code, Eindhoven University of Technology, Power and Flow.

[35] F. Liu, J.-L. Consalvi, P.J. Coelho, F. Andre, M. Gu, V. Solovjov, B.W. Webb, The impact of radiative heat transfer in combustion processes and its modeling with a focus on turbulent flames, Fuel 281 (2020) 118555.